Modelling He and H Isotopes in the Radiation Belts

R.S. Selesnick and R.A. Mewaldt

California Institute of Technology, Pasadena, California

Nuclear interactions between inner zone protons and atoms in the upper atmosphere produce energetic H and He nuclei that are an additional radiation belt source. We calculate production rates of these isotopes from models of the inner zone proton intensity, the upper atmosphere drift averaged composition and densities, and cross-sections for the various interaction processes. For comparison with observations of radiation belt H and He isotopes, the production rates are combined with a model of the energy loss rate in the residual atmosphere to calculate particle intensities. Although the calculations are in principle straightforward, they depend on a detailed knowledge of the various model inputs, including models for radiation belt protons, and may also depend on the phase of the solar cycle. On the other hand, the results of the calculations, when compared with the observational data, can provide useful tests of the model inputs. Preliminary results show that the atmosphere is a significant source for inner zone ^{4}He, ^{3}He, and d.

1. INTRODUCTION

The inner radiation belt is composed primarily of protons that were produced locally by the cosmic ray albedo neutron decay (CRAND) process, due to collisions between cosmic rays and the neutral atmosphere. The trapped protons similarly create a secondary source of trapped particles by their own nuclear interactions with the atmosphere. This process is less efficient than CRAND for producing protons because the particles must be injected directly whereas the neutrons can propagate to high altitudes, where the atmospheric density is low, before decaying. However, because CRAND produces only protons and electrons, the secondary process can be a significant source of other trapped particles such as isotopes of H and He.

The CRAND source has been the subject of several theoretical calculations for comparison with the trapped proton data (e.g. *Dragt* [1971]; *Farley and Walt* [1971]; *Jentsch and Wibberenz* [1980]; *Jentsch* [1981]). However, probably due to a lack of data on the composition of the high energy trapped ions, the secondary source has not been studied in detail. The new data from SAMPEX [*Cummings et al.*, 1995; *Looper et al.*, 1995] prompted us to begin such an investigation. Although the calculation is analogous to the CRAND case, it is complicated by the need to calculate the source function due to each of the many possible nuclear interactions. In the CRAND calculations the neutron source was generally an empirical model based on neutron flux measurements.

2. CALCULATIONS

If the atmospheric production of trapped particles is balanced only by ionization energy loss in the atmosphere, then their intensity j satisfies a continuity equation [*Jentsch and Wibberenz*, 1980]

$$\frac{1}{v}\frac{\partial j}{\partial t} = S + \frac{\partial}{\partial E}\left(j\left|\frac{dE}{dx}\right|\right) , \qquad (1)$$

where $v = dx/dt$ is the (non-relativistic) speed of the trapped particle at time t and kinetic energy E. The production rate in $(\mathrm{cm^3 s\ sr\ MeV})^{-1}$ is S. The intensity j can be time dependent through S which generally varies due to the solar cycle. In the steady-state case, or if the particle lifetimes are short

Radiation Belts: Models and Standards
Geophysical Monograph 97

compared to the 11 year solar cycle, the solution is

$$j = \frac{1}{\left|\frac{dE}{dx}\right|} \int_E^\infty S\, dE\,. \tag{2}$$

The integral should be cut-off at the maximum energy of adiabatically trapped particles, but this is not significant for a sufficiently soft spectrum. The solution (2) also applies to particles with lifetimes that are long compared to the solar cycle time if S is interpreted as the solar cycle average value. For cases where the lifetimes are comparable to the solar cycle time, a time dependent solution is possible [*Jentsch and Wibberenz*, 1980]. For protons, the continuity equation (1) is valid for low L shells ($L \lesssim 1.3$) beyond which radial diffusion from an external source becomes significant at low energies ($\lesssim 30$ MeV) [*Jentsch*, 1981].

The production rate of secondaries is

$$S = \sum_i \int dE_\mathrm{p} \int d\Omega_\mathrm{p}\, n_i j_\mathrm{p} \frac{d^2\sigma_i}{d\Omega dE}\,. \tag{3}$$

The summation extends over all interactions that lead to a given type of secondary particle and the integrals cover the range of proton energies E_p and solid angle Ω_p that kinematically can produce secondaries with energy E, pitch-angle α in a solid angle Ω, and at a given L shell. The atmospheric density, n_i, of target atoms for the interaction i is averaged over the drift path of protons for each L and proton pitch angle α_p. The proton intensity is j_p and the cross section for interaction i is σ_i. Both n_i and j_p may be functions of time due to solar cycle variations. Calculating S from Eq. (3) requires knowledge of the atmospheric densities, the trapped proton intensities and drift paths, and the interaction cross-sections. In addition, calculating j from (3) requires knowledge of the energy loss rate in the atmosphere.

For the atmosphere we use the Mass-Spectrometer-Incoherent-Scatter-1986 (MSIS-86) neutral atmosphere model [*Hedin*, 1987] as encoded by the National Space Science Data Center (NSSDC), which provides number densities of He, O, N_2, O_2, Ar, H, and N as functions of day-of-year, local time, altitude, geodetic latitude and longitude, solar 10.7 cm flux ($F_{10.7}$) for the previous day and a 3 month average, and the magnetic A_p index. For the Earth's magnetic field we use the International Geomagnetic Reference Field (IGRF) model extrapolated to 1992 [*Langel*, 1991] from the NSSDC. To calculate the drift averaged densities for each element, trajectories of 100 MeV protons were calculated numerically for a given L shell starting from the minimum magnetic field B on that L shell at a given altitude and continuing for one complete drift in longitude around the Earth. The minimum B was converted to an equatorial pitch angle and the starting altitude was varied to provide the drift-averaged densities as a function of α_p. A typical value of $F_{10.7} = 140$ was used to simulate solar average conditions.

The drift averaged atmospheric densities were also used to calculate energy loss rates in the atmosphere using the formulas compiled by *Salamon* [1980]. We assume that the secondary particles have no bound electrons. Note that for $L \gtrsim 1.3$ energy loss to free electrons in the ionosphere and plasmasphere can be significant [*Jentsch*, 1981], but this is not included in the model. Trapped particle lifetimes against energy loss in the atmosphere can be calculated from dE/dx. They are generally short at low altitudes (small equatorial pitch-angles) but can be long at high altitudes and L shells. Note that the trapped particles observed by a satellite orbiting at low altitude must all have relatively short lifetimes regardless of L shell because all of these particles must reach that altitude.

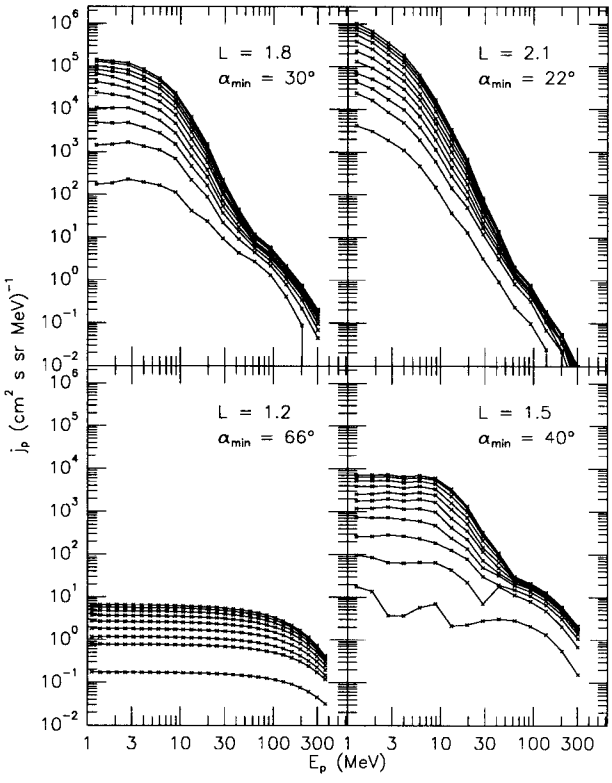

Figure 1. Proton energy spectra for selected L shells from the AP-8 model for solar average conditions. The curves for each L are at equally spaced pitch angles varying from the labeled minimum α to 90°. Some smoothing was done for the $L = 1.2$ curves.

The proton intensities were derived from the empirical NASA AP-8 models obtained from NSSDC. These provide proton omnidirectional integral intensities, J_p, as a function of L and B/B_0, the ratio of local to equatorial magnetic fields, for solar minimum and solar maximum conditions, although significant solar cycle variations were not found for our region of interest. The equatorial directional differential intensity was calculated by numerically evaluating

$$j_p = \frac{1}{2\pi^2} \frac{\partial^2}{\partial E\, \partial x} \int_0^x \frac{J_p(E, x')}{(x - x')^{1/2}}\, dx'\,, \tag{4}$$

where $x = B_0/B$. Sample proton energy spectra are shown in Figure 1.

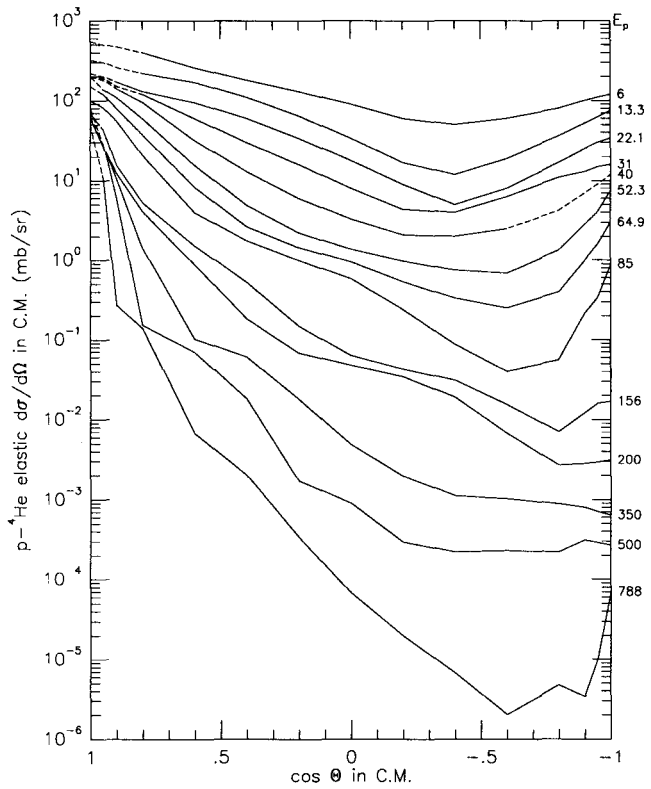

Figure 2. Cross-sections versus scattering angle in the center-of-mass for p-^{4}He elastic scattering [*Meyer*, 1972; *Votta et al.*, 1974; *Comparat et al.*, 1975; *Fong et al.*, 1978; *McCamis et al.*, 1978; *Imai et al.*, 1979; *Moss et al.*, 1980]. Dashed curve segments are extrapolations from the data. Laboratory proton energies are labeled to the right of each curve in MeV.

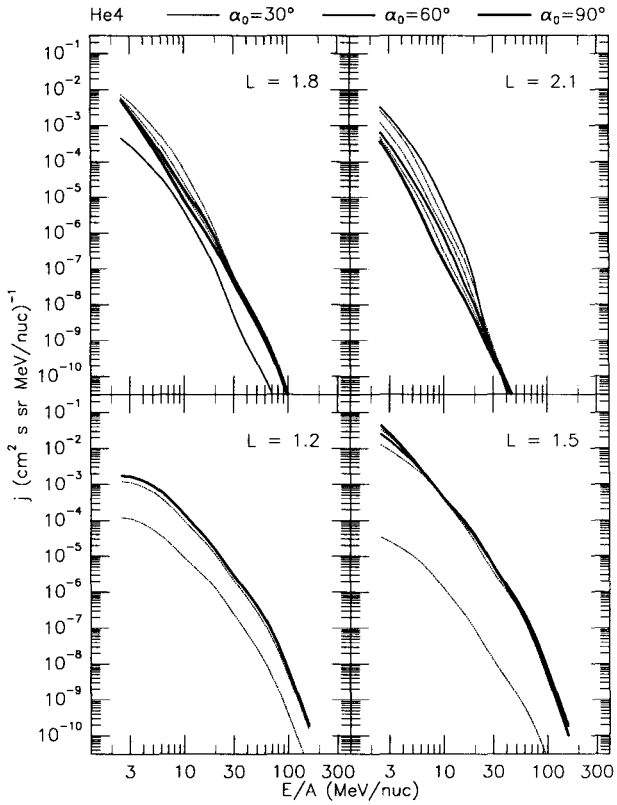

Figure 3. Intensity of elastically scattered ^{4}He as a function of energy-per-nucleon at average solar conditions for the labeled L shells. The equatorial pitch angles α_0 vary from 30° (off scale for low L) to 90° in steps of 10°.

The final input to the source function (3) is the cross-section data for a given nuclear interaction. This should be differential in energy and solid-angle. If the interaction has only two in-going and two out-going particles then the kinematics can be used to simplify the calculation. For the reaction designated 1(2,3)4 involving particles of rest mass m_1, m_2, m_3, and m_4, where m_1 collides with m_2 which is at rest in the laboratory system, the initial 4-momenta are $(E_1, \mathbf{p}_1)$, $(m_2, 0)$ in the lab and $(\varepsilon_1, \mathbf{k})$, $(\varepsilon_2, -\mathbf{k})$ in the center-of-mass, while the final 4-momenta are $(E_3, \mathbf{p}_3)$, $(E_4, \mathbf{p}_4)$ and $(\varepsilon_3, \mathbf{k}')$, $(\varepsilon_4, -\mathbf{k}')$ respectively. If m_4 is the secondary particle of interest, then the scattering angles in the center-of-mass, Θ, and the lab, θ_4 are related to the energies by the Lorentz transformation

$$E_4 = \gamma\varepsilon_4 - \gamma\beta k' \cos\Theta \tag{5}$$

and to each other by

$$\tan\theta_4 = \frac{\sin\Theta}{\gamma(-\cos\Theta + \frac{\beta}{\beta_4})}, \tag{6}$$

where $\beta = p_1/(\gamma E)$ and $\gamma = (E_1+m_2)/E$ are the center-of-mass speed and Lorentz factor, $E = (2E_1m_2+m_1^2+m_2^2)^{1/2}$ and $\beta_4 = k'/\varepsilon_4$ are the total energy and m_4 speed in the center-of-mass. From Eq. (5)

$$\frac{d\sigma}{dE_4} = -\frac{2\pi}{\gamma\beta k'}\frac{d\sigma}{d\Omega_c}, \tag{7}$$

where Ω_c is the center-of-mass solid angle. In this case the double differential cross-section can be expressed in terms of either of the single differential cross-sections. For example

$$\frac{d^2\sigma}{d\Omega dE_4} = \frac{d\sigma}{dE_4}\frac{\delta(\theta_4 - \theta_4(E))}{2\pi\sin\theta_4} \tag{8}$$

where $\theta_4(E)$ is given by Eq. (6).

To do the source integral (3) over the δ-function in Eq. (8) we change variables from α_p and the proton gyrophase angle to θ and the initial proton phase angle ϕ_p around the secondary particle direction, by a rotation of the axes:

$$S = \sum_i \int dE_p \frac{d\sigma_i}{dE}\frac{1}{\pi}\int_0^\pi d\phi_p\, n_i j_p, \tag{9}$$

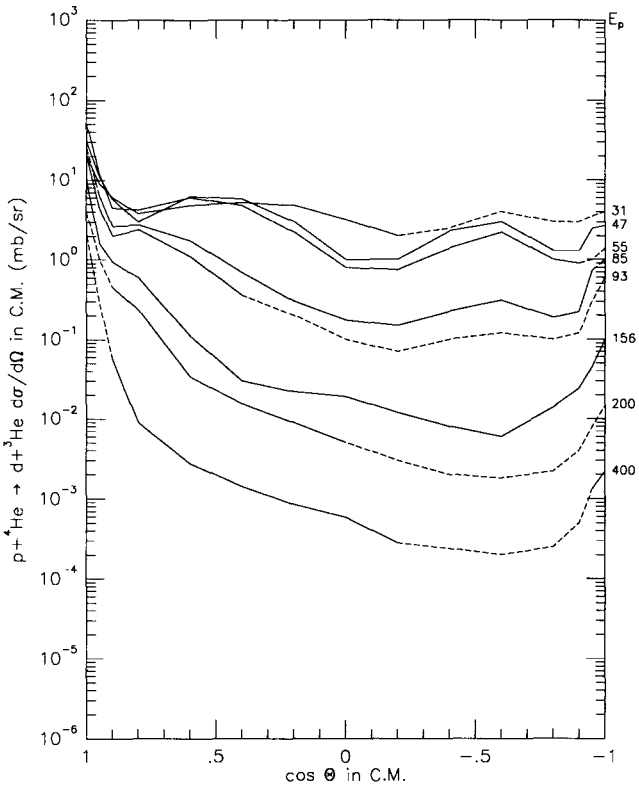

Figure 4. Cross-sections versus scattering angle in the center-of-mass for the reaction $p+^4He \rightarrow ^3He+d$ [*Meyer*, 1972; *Votta et al.*, 1974; *Alons et al.*, 1986]. Dashed curve segments are extrapolations from the data. Laboratory proton energies are labeled to the right of each curve in MeV.

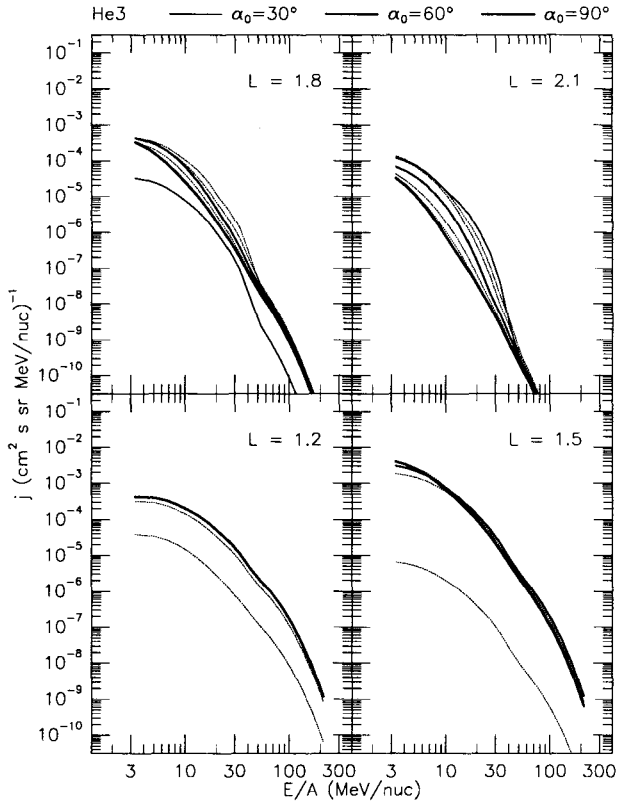

Figure 5. Similar to Figure 3 but for ^3He from the reaction $p+^4He \rightarrow ^3He+d$.

where $\cos\phi_p = (\cos\alpha_p - \cos\alpha\cos\theta)/(\sin\alpha\sin\theta)$ and θ is the scattering angle θ_4 from Eq. (6). Note that if n_i and j_p are independent of α_p then (9) leads to the expected result

$$S = \sum_i \int dE_p n_i j_p \frac{d\sigma_i}{dE} \qquad (10)$$

for the source function due to an isotropic proton flux in a homogeneous atmosphere.

The first interaction that we consider is $p(^4He,p)^4He$, elastic scattering of atmospheric ^4He. The maximum kinetic energy of the scattered ^4He is approximately 16/25 times the proton kinetic energy, so that a 100 MeV proton can produce a ^4He of up to 16 MeV/nucleon. Cross-section data are shown in Figure 2 from various sources listed in the figure caption. They are generally peaked in the direction where protons are forward scattered, but the most efficient direction for trapping the scattered ^4He is where the protons are scattered backward ($\cos\Theta = -1$), and the scattered ^4He follow the original proton trajectories. However, small and intermediate angle scattering can also lead to significant particle trapping if the pitch angle is approximately conserved, especially at the high proton energies where the cross-sections are strongly forward-peaked.

Results of the calculation using Eqs. (9) and (2) for elastic scattering of ^4He are shown in Figures 3. The ^4He intensity at a given energy-per-nucleon varies with equatorial pitch angle due the corresponding variation in the relative concentration of ^4He in the drift-averaged atmosphere. It varies with L primarily due to the variation in the proton intensity. The pitch angle distribution changes from being strongly peaked at 90° for $L = 1.2$ to being peaked near the edge of the loss cone for $L = 2.1$.

We next consider the pickup reaction $p(^4He,d)^3He$. Cross-section data are shown in Figure 4. The backward direction ($\cos\Theta = -1$) is again most efficient for trapping ^3He while the forward direction ($\cos\Theta = 1$) is most efficient for trapping d. The ^3He and d intensities are shown in Figures 5 and 6 respectively.

The ^3He has a harder spectrum than the ^4He from elastic scattering due to the differing energy dependencies of the cross sections at backward angles. The deuterium intensity is much higher than those of ^4He and ^3He because the cross sections are forward peaked.

There are other reactions that can also produce the isotopes considered above. For example, protons can collide with atmospheric O, which is relatively dense at low altitudes, producing evaporation and direct knock-out products including

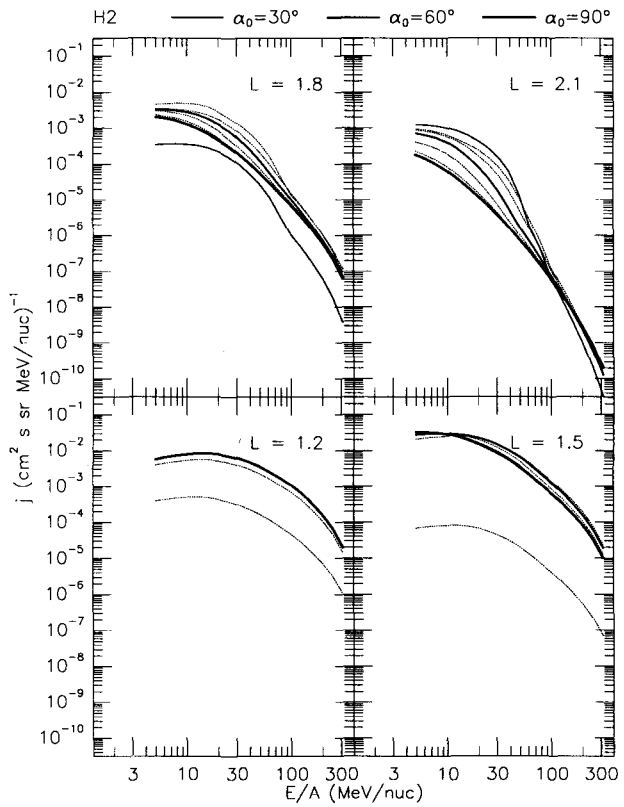

Figure 6. Similar to Figure 3 but for d from the reaction p + ^{4}He → ^{3}He + d.

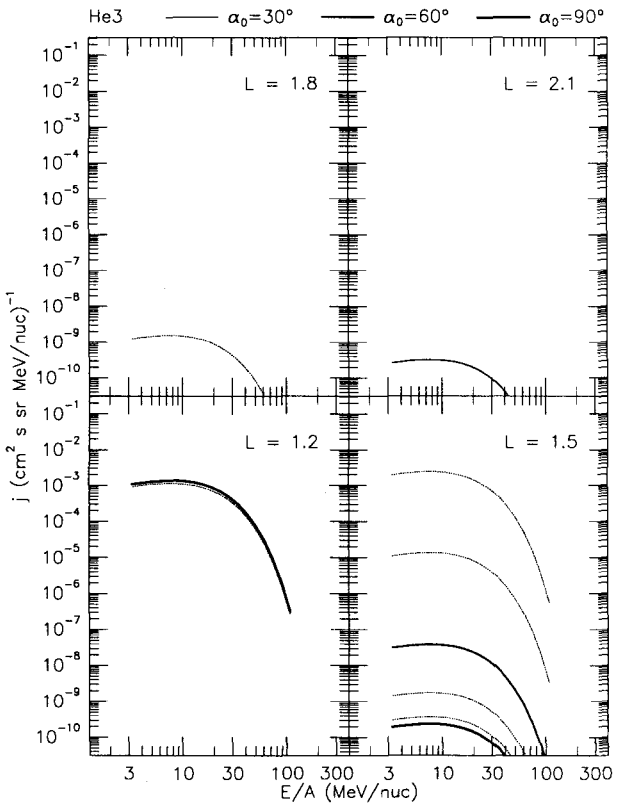

Figure 7. Similar to Figure 3 but for ^{3}He production by p knockout from O.

^{4}He, ^{3}He, and d. The kinematics are not determined as in Eq. (5). Instead, cross-sections and the energy distribution of the products are measured. However, the data are sparse and several approximations must be made. Detailed measurements at $E_p = 90$ MeV have been made by *Wu et al.* [1979]. They found that the evaporation products are generally isotropic and low-energy, so they are not significant here, while the knock-out products are forward-peaked and higher energy. To simplify the calculation we assume that they are produced in the forward direction only:

$$\frac{d^2\sigma}{d\Omega dE} = \sigma(E_p)\frac{\delta(\theta)}{2\pi \sin\theta}F(E_p, E)\,. \qquad (11)$$

For the energy distribution F we assume an exponential independent of E_p except for a cutoff at the maximum energy E_{max} which differs from E_p by the binding energy of the knock-out product in the original nucleus

$$F(E_p, E) = \frac{1}{E_0}\frac{e^{-E/E_0}}{1 - e^{-E_{max}/E_0}}H(E_{max} - E)\,. \qquad (12)$$

The e-folding energy is E_0 and H is a unit step function. The values of E_0 are taken from the angle-integrated spectra of Wu et al. and are 15.9 MeV for ^{4}He, 29.5 MeV for ^{3}He, and 77.8 MeV for d. The total cross sections $\sigma(E_p)$ are taken from *Cucinotta et al.* [1996].

The source function based on the approximation Eq. (11) is

$$S = \int dE_p n j_p \sigma F\,, \qquad (13)$$

where n, the drift averaged O density, and j_p are evaluated at $\alpha_p = \alpha$. The resulting ^{3}He intensities are shown in Figure 7. Atmospheric O appears to be a significant source at $L = 1.2$ only. At the higher L shells the O products are significant only in a narrow range of equatorial pitch angles near the edges of the loss cones, corresponding to the altitude range where O is the dominant component of the atmosphere. Similar results are obtained for d and ^{4}He. However, because of the differing energy spectra (different values of E_0) the atmospheric O source is relatively more significant for d and less significant for ^{4}He, compared with ^{3}He. Compared with the atmospheric He source at $L = 1.2$, atmospheric O appears to be a comparable source of ^{4}He and d, and a dominant source of ^{3}He. However, the O source is uncertain due to the lack of cross-section data and should be considered only a rough estimate.

3. DISCUSSION

The ^{4}He, ^{3}He, and d intensities described above are comparable in magnitude to the results from SAMPEX reported by *Cummings et al.* [1995] and *Looper et al.* [1995], and to the higher energy CRRES data reported by *Wefel et al.* [1995]. Detailed comparisons between the data and model results will be reported elsewhere. However, it is clear that the atmosphere is a significant and possibly dominant source of these isotopes for the inner zone.

While the elastic scattering and pick-up reactions involving atmospheric He are reasonably well understood, the primary uncertainty in the calculations is due to the lack of experimental cross-section data for the reactions with atmospheric O. Other reactions may also be significant, such as p(p,d)π for producing high energy d, while elastic scattering of atmospheric constituents other than He, such as H and O, may also be significant sources for their corresponding radiation belt components.

Other possible improvements in the calculation would be to include solar-cycle variations, to evaluate the time dependence in cases where the lifetimes are comparable to the solar cycle time [*Jentsch and Wibberenz*, 1980], and to evaluate the role of radial diffusion, which is probably significant at the higher L shells [*Jentsch*, 1981].

Acknowledgements. This work was supported by NASA under contract NAS5-30704 and grant NAGW-1919.

REFERENCES

Alons, P.W.F., J.J. Kraushaar, J.R. Shepard, J.M. Cameron, D.A. Hutch-eon, R.L. Liljestrand, W.J. McDonald, C.A. Miller, W.C. Olsen, J.R. Tinsley and C.E. Stronach, ^{4}He(p,d)^{3}He reaction at 200 and 400 MeV, *Phys. Rev., C33*, 406–411, 1986.

Comparat, V., R. Frascaria, N. Fujiwara, N. Marty, M. Morlet, P.G. Roos and A. Willis, Elastic proton scattering on ^{4}He at 156 MeV, *Phys. Rev., C12*, 251–255, 1975.

Cucinotta, F.A., L.W. Townsend, J.W. Wilson, J.L. Shinn, G.D. Badhwar and R.R. Dubey, Light ion components of the galactic cosmic rays: nuclear interactions and transport theory, *Adv. Space Res., 17*, (2)77–(2)86, 1996.

Cummings, J.R, R.A. Mewaldt, R.S. Selesnick, E.C. Stone, J.B. Blake and M.D. Looper, MAST observations of high enery trapped helium nuclei (abstract), *EOS Trans. AGU*, Fall Meeting, F501, 1995.

Dragt, A.J, Solar cycle modulation of the radiation belt proton flux, *J. Geophys. Res., 76*, 2313–2244, 1971.

Farley, T.A. and M. Walt, Source and loss processes of protons in the inner radiation belt, *J. Geophys. Res., 76*, 8223–8241, 1971.

Fong, J., T.S. Baeur, G.J. Igo, G. Pauletta, R. Ridge, R. Rolfe, J. Soukup, C.A. Whitten, Jr., G.W. Hoffmann, N. Hintz, M. Oothoudt, G. Blanpied, R.L. Liljestrand and T. Kozlowski, p-^{4}He Elastic scattering at 788 MeV, *Phys. Lett., 78B*, 205–208, 1978.

Hedin, A.E., MSIS-86 thermospheric model, *J. Geophys. Res., 92*, 4649–4662, 1987.

K. Imai, K. Hatanaka, H. Shimizu, N. Tamura, K. Egawa, K. Nisimura, T. Saito, H. Sato and Y. Wakuta, Polarization and cross section measurements for p-^{4}He elastic scattering at 45, 52, 60, and 65 MeV, *Nucl. Phys., A 325*, 397–407, 1979.

Jentsch, V. and G. Wibberenz, An analytic study of the energy and pitch angle distribution of inner-zone protons, *J. Geophys. Res., 85*, 1–8, 1980.

Jentsch, V., On the role of external and internal source in generating energy and pitch angle distributions of inner-zone protons, *J. Geophys. Res., 86*, 701–710, 1981.

Langel, R.A., International geomagnetic reference field, 1991 revision, *J. Geomag. Geoelectr., 43*, 1007–1012, 1991.

M.D. Looper, J.B. Blake, Cummings, J.R, R.A. Mewaldt and R.S. Selesnick, Maps of hydrogen isotopes at low altitudes in the inner zone of the earth's magnetosphere (abstract), *EOS Trans. AGU*, Fall Meeting, F501, 1995.

McCamis, R.H., J.M. Cameron, L.G. Greeniaus, D.A. Hutch-eon, C.A. Miller, M.S. de Jong, B.T. Murdoch, W.T.H. van Oers, J.G. Rogers and A.W. Stetz, Large angle cross sections and analyzing power for proton-^{4}He elastic scattering between 185 and 500 MeV, *Nucl. Phys., A 302*, 388–400, 1978.

Meyer, J.P., Deuterons and He^3 formation and destruction in proton induced spallation of light nuclei ($Z < 8$), *Astron. Astrophys. Suppl., 7*, 417–467, 1972.

Moss, G.A., L.G. Greeniaus, J.M. Cameron, D.A. Hutch-eon, R.L. Liljestrand, C.A. Miller, G. Roy, B.K.S. Koene, W.T.H. van Oers, A.W. Stetz, A. Willis and N. Willis, Proton-^{4}He elastic scattering at intermediate energies, *Phys. Rev., C 21*, 1932–1943, 1980.

Salamon, M.H., A range-energy program for relativistic heavy ions in the region $1 < E < 3,000$ MeV/amu, Lawrence Berkeley Laboratory, University of California, 1980.

Votta, L.G., P.G. Roos, N.S. Chant and R. Woody, III, Elastic protons scattering from ^{3}He and ^{4}He and the ^{4}He(p,d)^{3}He reaction at 85 MeV, *Phys. Rev., C 10*, 520–528, 1974.

Wefel, J.P., J. Chen, J.F. Cooper, T.G. Guzik and K.R. Pyle, The isotopic composition of geomagnetically trapped helium, *Proc. Int. Cosmic Ray Conf.*, 24th (4), 1021–1024, 1995.

Wu, J.R., C.C. Chang and H.D. Holmgren, Charged-particle spectra: 90 MeV protons on ^{27}Al, ^{58}Ni, ^{90}Zr, and ^{209}Bi, *Phys. Rev., C 19*, 698–713, 1979.

R.S. Selesnick, R.A. Mewaldt, California Institute of Technology, Pasadena, CA 91125, USA

DISCUSSION

Q: J.B. Blake. Has tritium abundance been calculated?
A: R.S. Selesnick. No.
Q: J.B. Blake. Do you understand why we don't see tritium in the PET data?
A: R.A. Mewaldt. The available cross sections suggest that ^{3}H should be at least an order of magnitude less abundant than ^{2}H. It may be there in the data but not resolved.